Plastic strain is a mixture of avalanches and quasireversible deformations: Study of various sizes

Péter Szabó,* Péter Dusán Ispánovity, and István Groma

Department of Materials Physics, Eötvös University Budapest, H-1518 Budapest POB 32, Hungary

(Received 12 August 2014; revised manuscript received 11 December 2014; published 13 February 2015)

The size dependence of plastic flow is studied by discrete dislocation dynamical simulations of systems with various amounts of interacting dislocations while the stress is slowly increased. The regions between avalanches in the individual stress curves as functions of the plastic strain were found to be nearly linear and reversible where the plastic deformation obeys an effective equation of motion with a nearly linear force. For small plastic deformation, the mean values of the stress-strain curves obey a power law over two decades. Here and for somewhat larger plastic deformations, the mean stress-strain curves converge for larger sizes, while their variances shrink, both indicating the existence of a thermodynamical limit. The converging averages decrease with increasing size, in accordance with size effects from experiments. For large plastic deformations, where steady flow sets in, the thermodynamical limit was not realized in this model system.

DOI: 10.1103/PhysRevB.91.054106 PACS number(s): 61.72.Lk, 81.40.Lm, 83.50.−v

I. INTRODUCTION AND OVERVIEW

Recent experiments reveal that the stress-strain curve of micrometer-scale specimens contains random steps, where the plateaus mark sudden strain bursts caused by dislocation avalanches [1–6]. The corresponding microscopic mechanism is as follows: as the stress increases, dislocations bow out from their equilibrium positions. At a sufficiently high local stress, a dislocation escapes (unpins) and quickly travels through the crystal and produces plastic strain. This event leads to the redistribution of internal stresses and may activate further dislocations. The strain burst is this resulting collective motion and it lasts until all participating dislocations settle in a new equilibrium position. This mechanism is best observable in the stress-strain response of micrometer-scale samples [7]. According to acoustic emission measurements, however, the plastic deformation of macroscopic specimens is also accumulated in numerous such local events [1,8]. Since as the system size increases the plastic strain increment corresponding to a local event tends to zero [4,6,9], the stress-strain curve of macroscopic bodies is continuous without exhibiting any apparent random steps.

Most of the plastic strain, therefore, is accumulated during strain bursts, but not all of it. As mentioned above, dislocations bow up already before unpinning, so some plasticity occurs in the ramp up regime (that is, between strain bursts), too. This process is reversible: if the applied stress was reduced, dislocations would move back to their original positions, and the corresponding plastic strain would disappear. From a macroscopic viewpoint, this effect cannot be distinguished from elasticity, and it manifests in the apparent change in the elastic constants, like Young's modulus. This phenomenon was first identified by Lawson [10] for polycrystalline copper in 1941, with an explanation later proposed by Eshelby [11]. The numerous investigations that followed on a wide range of metals lead to the conclusion that during deformation Young's modulus drops around 10% at a strain of $\varepsilon \approx 10\%$ and then slowly increases [12,13]. Similar behavior is observed for the shear modulus with a maximum drop of ≈15%. This was explained as follows: after the heat treatment, most of the dislocations are pinned, so the bow out phenomenon is weak. During stage I of deformation, a large number of moving dislocations are generated with long unpinned segments, so the amount of "elastic plasticity" increases and the elastic moduli drop. In stage II and later, cross-slip introduces new pinning points, leading to smaller amount of bow-out, and increasing moduli. The phenomenon that dislocation motion occurs below the flow stress was observed recently by Ispánovity *et al.* [14,15] in terms of micropillar compression experiments and discrete dislocation dynamics (DDD) simulations both in 2D and 3D.

As mentioned above, the stress-stain curve changes dramatically with system size: random steps appear for specimens in the mircometer range and below. In addition, size effects are observable already for larger samples: in most cases, the smaller sample requires higher stresses to get the same deformation [2,16]. The effect is traditionally modeled by phenomenological "nonlocal continuum" theories in which an appropriate gradient term is added to the stress-strain relation [17,18], or by continuum theories of dislocations [19–25]. It is obvious, however, since a continuum theory is an average and deterministic description, it is unable to account for the random steps on the stress-strain curves. To study the random character of plastic response, therefore, numerous large scale DDD [26–29] simulations were also employed, many focusing on the statistics of avalanches and its dependence on the sample size [6,30–32].

In this paper, we concentrate on the "elastic plastic" behavior described above in terms of DDD simulations in 2D and 3D. To this end, we perform quasistatic stress loading of dislocation ensembles and measure the accumulated deformation. Note that elastic deformations are not considered in this model, so strain and deformation are understood as purely plastic. Our main observations in this work are as follows. Between avalanches the deformation grows almost linearly with the stress. Tests of load cycles show that here the deformation is approximately reversible, so plasticity appears as a randomly alternating sequence of quasireversible deformations and avalanches. The slope of the linear regimes

*pszabo@metal.elte.hu

λ varies randomly for different realizations of systems of the same size. The system size dependence of our results is demonstrated in 2D simulations with different total number of dislocations N. We find a sharpening distribution for λ with increasing N. The full individual staircaselike stress-strain curves of the same N also have a mean that is a smooth function but it also depends on N'. Up to a certain threshold deformation γ_{th}, the mean stress-strain curve seems to converge for large N, with variance going to zero with increasing N. So, for large N, essentially the same continuous stress-strain curve emerges for each realization, indicating the existence of a thermodynamic limit. This refines the finding of Tsekenis *et al.* [31], where the natural scaling by $\sqrt{N}$ lets curves collapse even for smaller N. Within the region of thermodynamical limit $\gamma < \gamma_{\text{th}}$, for two decades in the strain, the mean stress-strain curve is a power law, with an exponent decreasing from 1 for small N to about 0.8 for large N. This is caused by the alternation of linear, quasireversible segments and plateaus of avalanches with random lengths in the stress-strain response function. Furthermore, for the 2D model under study, there seems to be no thermodynamical limit for large deformations.

II. SIMULATION METHOD

Plastic deformation is mainly due to the motion of dislocations [33], interacting via a long-range stress field. Here, we first apply one of the simplest 2D models of dislocation systems that has been used extensively in the literature [1,34–37]. In spite of its simplicity, the model described below contains the following fundamental properties of dislocations: (i) they interact via anisotropic long-range $(1/r)$ stress fields, (ii) their motion is dissipative due to phonon drag, and (iii) they can only move in certain directions determined by the crystallographic slip systems. An additional advantage of the model lies in the fact that there are no fitting parameters present in it. Since several dislocation mechanisms, like interaction with forest dislocations, cross-slip, or dislocation creation are neglected, the direct applicability of the model should be constrained to study stage I deformation at low temperatures. To date, however, the model has contributed to the understanding and description of quite a few dislocation-based phenomena, e.g., the shape of x-ray line profiles [38–40], strain burst size distributions [1,6], Andrade creep [41–43], and spatial dislocation correlations [44]. It also serves as a basis for developing continuum theories of dislocation dynamics [19,45].

In the model, straight and parallel edge dislocations with parallel slip axes are considered, essentially a 2D cross section of a 3D system. Periodic boundary conditions are used on a square of side L, the slip axes are parallel to one edge of the square (the x axis), and for each realization, dislocations are initially randomly placed with a uniform distribution. In the beginning, each realization contains a fixed number N of dislocations, with equal number of positive and negative Burgers vectors $s(b,0)$, where b is the lattice constant and $s = \pm 1$. Only dislocation glide along the x axis is taken into account so the dislocations' vertical (y) coordinates are constant.

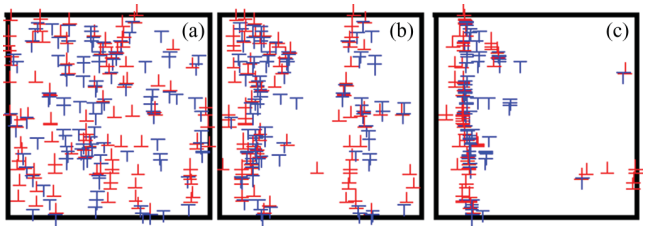

FIG. 1. (Color online) Typical configuration at (a) relaxed state without external stress ($\gamma = 0$), (b) relaxed in the presence of medium external stress ($\gamma \approx 1$), and (c) with external stress just below the steady flow ($\gamma \approx 1000$). The $\perp$ (red) and the $\top$ (blue) denote the $s = +/-$ signs, respectively.

One positive dislocation induces the shear stress field

$$\tau_{\text{ind}}(\vec{r}) = bDx(x^2 - y^2)/r^4, \tag{1}$$

where $\vec{r} = (x,y)$ is the radius vector from that dislocation, $r = |\vec{r}|$, $D = \mu/[2\pi(1-\nu)]$, with μ being the shear modulus and ν the Poisson number. The ith dislocation is exposed to the shear stress field of all the others $j \neq i$ and to the external field, taken to be the uniform τ_{ext}, wherein it performs overdamped motion with drag coefficient B. Thus the equation of motion of the ith dislocation is [14,43]

$$\dot{x}_i = B^{-1} b s_i \left[\sum_{\substack{j=1 \\ j \neq i}}^{N} s_j \tau_{\text{ind}}(\vec{r}_i - \vec{r}_j) + \tau_{\text{ext}} \right], \tag{2}$$

where the s_k is the sign of the kth dislocation and $\vec{r}_k = (x_k, y_k)$ its position. The plastic strain is calculated by $\gamma = b/L^2 \sum_i s_i \Delta x_i$, where Δx is the change in the x coordinate relative to the initial value. This equation is rendered periodic numerically by including sufficiently many mirror images of the jth dislocation. The resulting equation of motion is solved with the 4.5th-order Runge-Kutta method. Adaptive step size is used to better treat narrow dipoles. Since very narrow dipoles would demand excessive computation time, we annihilate (different sign) or merge (same sign) dislocations if they are closer than $0.05\,L/\sqrt{N}$. Whereas annihilation decreases the dislocation number, in order to avoid ambiguity, in the conversion formulas we use the original dislocation number N.[1] Note that dislocations are not created in our model, corresponding to non-source-controlled plastic deformations. Throughout the paper, simulations with $N = 32,64,128,256,512,1024,2048$ were considered with ensembles numbering $10^4, 3000, 2000, 800, 300, 100, 80$, respectively, and for the largest sizes our computational power allowed the scanning only of restricted regions of simulated strain. Typical dislocation configurations are seen in Fig. 1.

Equation (2) is represented in the computer by $B_{\text{cp}} = D_{\text{cp}} = b_{\text{cp}} = L_{\text{cp}} = 1$, yielding the density $\rho_{\text{cp}} = N/L_{\text{cp}}^2 = N$. The mapping to different sample sizes, while the physical

[1]It was checked that decreasing the annihilation distance does decrease the amount of annihilation events, but does not change the results presented in this paper.

dislocation density is kept constant, occurs by our introduced natural quantities $\gamma = \gamma_{\rm cp}/\sqrt{N}$, $\tau = \tau_{\rm cp}/\sqrt{N}$, $x = x_{\rm cp}\sqrt{N}$, $t = t_{\rm cp}N$, used throughout this paper [35]. Then physical quantities are obtained from the physical density $\rho_{\rm ph}$ as $L_{\rm ph} = \sqrt{N/\rho_{\rm ph}}$, $\gamma_{\rm ph} = \gamma b_{\rm ph}\sqrt{\rho_{\rm ph}}$, $\tau_{\rm ph} = \tau b_{\rm ph} D_{\rm ph}\sqrt{\rho_{\rm ph}}$, $t_{\rm ph} = t B_{\rm ph}/(b_{\rm ph}^2 D_{\rm ph}\rho_{\rm ph})$. To give an example, if on the natural scale $\gamma = 0.35$ then for the generic physical variables $\rho_{\rm ph} = 2 \times 10^{14}$ m^{-2} and $b_{\rm ph} = 2$ Å, we would obtain the physical deformation $\gamma_{\rm ph} = 0.1\%$.

In the scenario presented here (identical to that of Refs. [30,31,46]), firstly, we let the system relax without external stress to form the initial state with $\gamma = 0$. Then we apply quasistatic stress loading, i.e., we increase the external stress by a small rate. The stress rate was chosen as low as possible yet computationally still affordable, $\dot{\tau}_{\rm ext} = 5 \times 10^{-5}$. The stress is increased so long as the mean absolute velocity of the dislocations remains under the threshold 5×10^{-4} (for a detailed discussion on the stress rate and the velocity threshold see Ref. [15]). If that threshold is surpassed (this is our definition of an avalanche) then the external stress is kept constant until the mean absolute velocity drops again below the threshold. The end state is a steady flow, that is, an infinite avalanche, because in the absence of dislocation creation no work hardening takes place for large deformations.

To generalize our findings, we also employ 3D DDD [47–51] to study the "elastic plastic" behavior caused by dislocation bow out. The simulations are identical to that of Ref. [15], so we summarize only some important details hereafter. Tensile loading of a cuboid-shaped Cu single crystal (micropillars) oriented for multiple slip (with [100] orientation) is carried out. The pillars exhibit a 3:1:1 aspect ratio and the loading direction is parallel to the longer edges (see Fig. 2). The length of the basal edges is 0.36 μm. The dislocation structure initially consists of Frank-Read sources of uniform length (0.2 μm) equally distributed among the possible slip systems. Since cross-slip is allowed, this configuration leads to a similar plastic response to those with more realistic arrangements [49]. The dislocation density was originally $\rho \approx 6 \times 10^{13}$ m^{-2}, which slightly increased during the tensile deformation. Quasistatic loading similar to the 2D case described above was implemented [15]. Further details on the algorithm can be found elsewhere [52]. Conducting simulations in 3D demands much higher computational time than in 2D, which even increases very sharply for larger specimen sizes. The study presented in this paper requires large ensembles of simulations with the same parameters, consequently, 3D simulations had to be limited to only one system size. It is noted that the results obtained by 3D DDD will be presented using physical units for stress and strain.

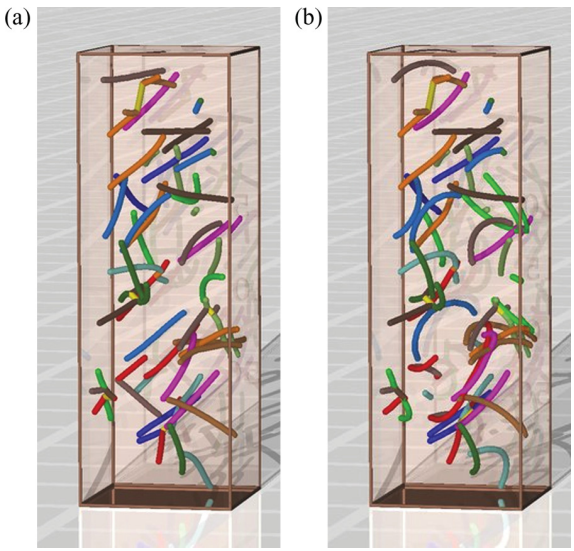

FIG. 2. (Color online) Typical configuration of 3D DDD simulations at (a) zero applied stress (and, thus, strain) and (b) just before the first avalanche sets on, where many dislocations are bowed out. Dislocation colors denote different glide planes of the fcc crystal structure.

III. INDIVIDUAL STRESS-STRAIN CURVES AND EFFECTIVE MOTION BETWEEN AVALANCHES

We first show typical dislocation configurations for various plastic deformations γ along our scenario in Fig. 1. Firstly, dislocations relax in the absence of external stress, forming a random-looking configuration of numerous smaller clusters, see Fig. 1(a). Due to the increasing external stress, the deformation γ generically increases, while clusters grow mainly in the y direction [Fig. 1(b)]. Beyond some threshold steady flow emerges, marked usually by a single dipolar wall, spanning across the whole simulation area [Fig. 1(c)], while one or two dislocations are circling quickly along their slip axes, in conformance to the periodic boundary conditions. Hence we must conclude that in the steady flow boundary effects are important, thus our model may not be realistic in this region, and so we concentrate our study to smaller deformations.

The plastic stress-strain curves $\tau_{\rm ext}(\gamma)$ of individual realizations are like staircases, they exhibit a sequence of plateaus of constant stress corresponding to avalanches, in accordance with earlier results [1–4,15,30], see Fig. 3. A novel observation here, to our knowledge not noted earlier, is that between plateaus, where the stress increases, the $\tau_{\rm ext}(\gamma)$ functions are

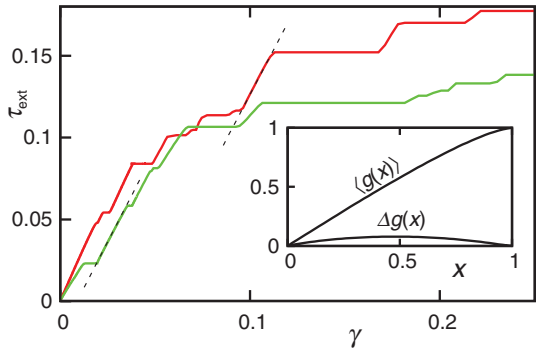

FIG. 3. (Color online) Stress-strain curves $\tau_{\rm ext}(\gamma)$ of two realizations obtained by 2D DDD with $N = 512$. Segments between plateaus are found to be nearly linear, dashed lines are guide to the eye. Inset: averages of increasing segments normalized as in Eq. (3) for fixed N's all fall on the same curve, close to a linear function. The lower arc is the standard deviation, again nearly independent on N.

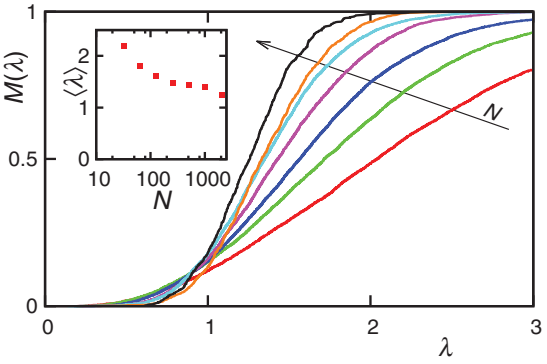

FIG. 4. (Color online) Cumulative probability distribution function $M(\lambda, N)$ of the steepness λ of the quasilinear segments for the 2D DDD simulations with system sizes $N = 32, 64, \ldots, 2048$ for $\gamma \leqslant 0.2$. The arrow points towards increasing N (colors distinguish sizes). Inset: the mean $\langle\lambda\rangle$ as functions of the system size N.

nearly linear. For the sake of comparison we normalized each increasing segment to a function $g(x)$ starting and ending at the opposite corners of the unit square as

$$g(x) = \frac{\tau_{\text{ext}}\left(x(\gamma_1 - \gamma_0) + \gamma_0\right) - \tau_0}{\tau_1 - \tau_0}, \quad x \in [0,1], \tag{3}$$

where γ_0, γ_1 and τ_0, τ_1 mark the borders of the chosen segment. Such normalized segments of individual runs with $\gamma < 0.2$ were separately averaged for fixed sizes N, and the resulting curves fall onto each other and form $\langle g(x)\rangle$ in the inset of Fig. 3. Here, also the standard deviation of the normalized segments is plotted, which is again nearly the same for various N's. So the segments between avalanches on the stress-strain curves, normalized according to Eq. (3), follow on the average a universal, nearly linear form, with a universal variance.

In order to test the properties of the close-to-linear segments, we ran a few loading cycles on individual realizations with various stress rates. In most of the cases, apart from a small, smooth, transient due to the finiteness of the stress rate, and from tiny avalanches, reversibility was found. Motivated by this "quasireversible" response, we surmise that deformations obey an effective equation of motion:

$$\dot{\gamma}(t) \approx -F(\gamma(t) - \gamma_0) + \tau_{\text{ext}}(t) - \tau_0, \tag{4}$$

where (γ_0, τ_0) is the endpoint of the last avalanche, where the system is assumed to be in equilibrium, and F is the effective restoring force, depending only on the increment $\gamma - \gamma_0$. Similarly as Eq. (3) associates $g(x)$ with the stress, we normalize the force $F(\gamma - \gamma_0)$ onto the unit square. Again, like

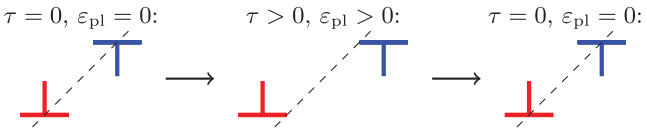

FIG. 5. (Color online) A dislocation dipole stretches when experiencing an applied shear stress (smaller than its yield stress), and meanwhile generates plastic strain. If the stress is released, the dislocations move back to their original position and the plastic strain disappears.

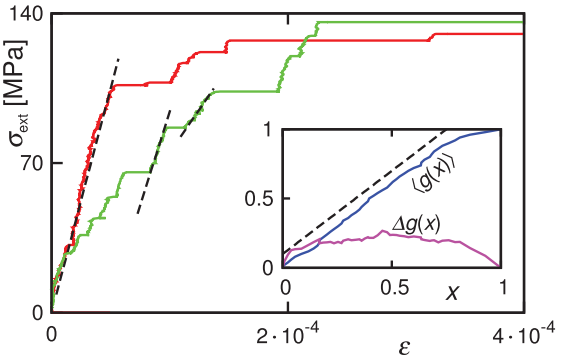

FIG. 6. (Color online) Equivalent to Fig. 3 for 3D DDD simulations.

the external stress in the inset of Fig. 3, the mean normalized force very weakly depends on N, and this universal function is astonishingly close to $g(x)$, which is the consequence of the low stress rate resulting $\dot{\gamma}(\gamma) \ll \tau_{\text{ext}}(\gamma)$. Thus even the force is very close to linear. We emphasize that near the equilibrium of a dislocation configuration, for small displacements, the elastic energy of course grows quadratically, so there the response should be linear. The remarkable feature in our case is that linearity holds way up to near the onset of the next avalanche. This instability is indeed marked by the slight curving of the universal function close to one in Fig. 3. Note that its slope there is not zero, whereas it would be zero in the case of a force-activated escape from a 1D potential, because of rare negative avalanches with $\dot{\gamma} < 0$.

To visualize the statistical nature of the quasireversible regions, in Fig. 4 we plot the cumulative probability distribution function $M(\lambda)$ of the steepness $\lambda = (\tau_1 - \tau_0)/(\gamma_1 - \gamma_0)$ for $\gamma \leqslant 0.2$ (chosen as a practical value). The curves visibly contract with increasing N, showing convergence to a finite mean. A nearly linear response here means that due to the interaction of dislocations, an effective shear modulus arises. The latter can be interpreted as the plastic component of the total empirical shear modulus in real crystals. Note that in the present model elastic deformations are not included.

The basic mechanism responsible for the plastic shear modulus λ is visualized in Fig. 5. A small enough applied

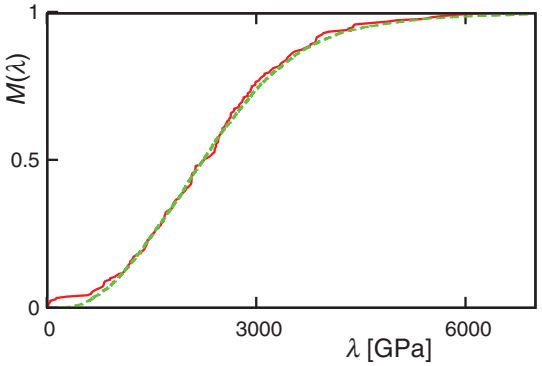

FIG. 7. (Color online) Equivalent to Fig. 4 for 3D DDD simulations. The dashed line is a rescaled version of the $M(\lambda)$ distribution from Fig. 4 for $N = 32$.

stress stretches the dipole and generates some plastic strain proportional to the dipole distance. If the stress is removed, dislocations move back to their original positions. The dislocation structure of Fig. 1 is of course more complex, but under stress it behaves in a similar manner. The emerging plastic shear modulus is related to the local structure or correlations of the dislocations (the smaller the average dipole distance is, the larger the modulus becomes).

The same analysis was performed for the 3D DDD simulations, too. Two typical stress-strain curves obtained are shown in Fig. 6. They also consist of horizontal plateaus corresponding to strain bursts, and interconnecting close to linear segments. During these ramp-up regimes, dislocations bow out as seen in Fig. 2(b). Averaging the $g(x)$ function [see Eq. (3)] leads to a linear function, slightly bending just before the onset of the next avalanche. This means that the general shape of the $g(x)$ function is the same either if it is due to dislocation bow out or the dipole-type mechanism of Fig. 5. The cumulative distribution of the linearity coefficients $M(\lambda)$ is plotted in Fig. 7, exhibiting a very similar shape to the 2D case.

IV. MEAN AND FLUCTUATION OF THE STRESS AS FUNCTION OF THE STRAIN

So far, we concentrated on the quasireversible segments between avalanches, now we turn to the global statistical behavior of stress-strain curves. Firstly, we plot the average $\langle\tau_{\rm ext}\rangle(\gamma,N)$ over ensembles with fixed N in Fig. 8. A main feature is the power law behavior over decades up to a strain approximately 0.05 and stress around 0.1 (see inset), with an exponent close to 1 for small sizes and decreasing with size to about 0.8. We can interpret this feature such that the nearly linear segments of the stress-strain curves are interrupted by the avalanche plateaus just in the way that an effective power function with a smaller-than-one exponent emerges. That is, avalanches soften the linearity of quasireversible segments and give rise statistically to a power law.

On physical scales, taking a lattice constant $b = 2$ Å, a dislocation density $\rho = 2 \times 10^{14}$ m^{-2}, $\gamma = 0.05$ corresponds to $\gamma_{\rm ph} \approx 0.015\%$. It is important to note that this value is much smaller than the $\gamma_{\rm ph} = 0.2\%$ threshold value customarily considered to be the yield strain in engineering practice. The fact that the power law arises way below the empirical yield value indicates the determining role of avalanches for much lower plastic strains than expected earlier. On the other hand, this is in a convincing agreement with fatigue experiments on single crystals that showed irreversibility already below the physical range of $\gamma_{\rm ph} = 0.01\%$ [53].

Another important property seen in Fig. 8 is that for $\gamma \lesssim 1$ the stress-strain curves seem to converge for large N, a criterion for the existence of a thermodynamical limit. On the other hand, for large strains, the $N \to \infty$ tendency is inconclusive from our simulation, the stress values may even diverge. For intermediate strains $1 \lesssim \gamma \lesssim 100$, the convergent bundle of the curves switches order for the sizes we considered. Note that for fixed strains $\gamma \lesssim 1$ the stresses decrease with N. As discussed earlier in connection with physical units, increasing N here can mean increasing size with constant dislocation density. Therefore larger stresses for smaller N's as in Fig. 8 can be interpreted as a version of the property "smaller is harder." We emphasize, however, that our model has periodic boundary conditions, thus pileups, commonly held responsible for this phenomenon [54], cannot develop. This tendency reverses for large strains, where the stress increases with N. In this region, however, where the configuration resembling a single wall forms, as seen in Fig. 1(c), we do not suggest that the model bears general relevance to real materials.

Given the fact that the stress-strain response for macroscopic crystals with a fixed orientation is a well-defined, sharp curve, it is expected that the variance vanishes with increasing size. Accordingly, a decreasing variance was observed in micropillar experiments by Uchic *et al.* [2]. To study this effect, we plotted in Fig. 9 the standard deviation $\Delta\tau_{\rm ext}(\gamma,N)$ of the stress for ensembles with fixed N for different strains. In the region $\gamma \lesssim 1$, where the mean stress converged with N (see Fig. 8), the standard deviation decreases. We tested a power law convergence by plotting $\Delta\tau_{\rm ext}(\gamma,N)\,N^{0.4}$ in the inset of Fig. 9, and indeed the collapse demonstrates that the deviation vanishes like $1/N^{0.4}$. Thus, recalling that we found a sharp limit for the average stress when $\gamma \lesssim 1$, we can conclude that in this region there is a thermodynamical limit. On the

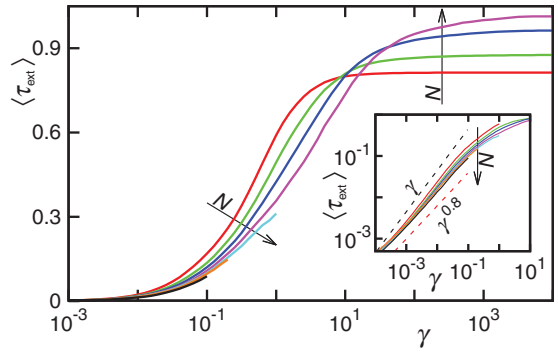

FIG. 8. (Color online) Mean stress $\langle\tau_{\rm ext}\rangle$ as a function of strain, for system sizes $N = 32,64,\ldots,2048$, for large N only smaller γ's were considered. Inset: log-log plot demonstrates the power law for $5 \times 10^{-4} \lesssim \gamma \lesssim 0.05$. The arrows point towards increasing N (colors distinguish sizes). The two dashed lines are guide to the eye.

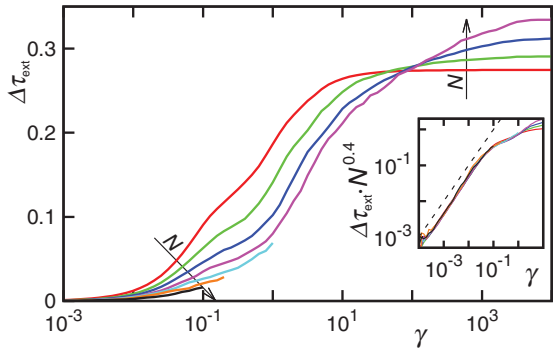

FIG. 9. (Color online) Standard deviation $\Delta\tau_{\rm ext}$ of the stress as function of the strain γ, for system sizes $N = 32,64,\ldots,2048$, for large N only smaller γ's were considered. The arrows point towards increasing N (colors distinguish sizes). Inset: log-log plot of $\Delta\tau_{\rm ext}\,N^{0.4}$ shows collapse, the dashed line with power unity is a guide to the eye.

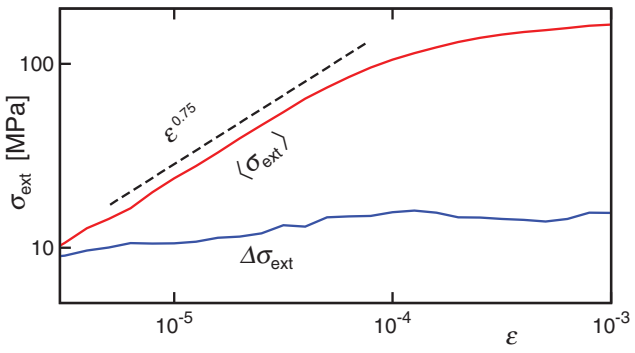

FIG. 10. (Color online) Mean stress $\langle\sigma_{ext}\rangle$ and standard deviation of the stress $\Delta\sigma_{ext}$ as a function of strain for 3D DDD simulations.

contrary, for large strains, Fig. 9 does not show convergence of the standard deviation, like there was no visible convergence of the mean in Fig. 8 either, so here the thermodynamical limit is absent. In the 3D DDD simulations, only one system size was studied but the shape of the average stress-strain curve and the stress fluctuations are very similar to the 2D case (see Fig. 10) [15].

V. CONCLUSION AND OUTLOOK

In this paper, our aim was twofold. On the one hand, we uncovered quasireversible behavior with nearly linear response between avalanches in models of simulated dislocations. For large sizes, the effective plastic modulus appears to converge in average. In the following, the obtained values are compared to the experimental observations. In case of shear modulus, the total reversible strain is

$$\gamma_{rev} = \gamma_{el} + \gamma_{pl,rev} = \mu^{-1}\tau + \lambda^{-1}\tau = (\mu^{-1} + \lambda^{-1})\tau, \quad (5)$$

so the effective shear modulus is $\mu_{eff} = (\mu^{-1} + \lambda^{-1})^{-1}$. In 2D, the limiting value is $\langle\lambda_{2D}\rangle \approx 1$ in the natural units introduced previously. It follows that in physical units, the plastic shear modulus is $\langle\lambda_{ph}\rangle = D_{ph}\langle\lambda\rangle$, that is, the resulting change in the elastic constants is ∼50%. In 3D, the plastic Young modulus is around 20 times higher than the elastic one, so $E_{eff} \approx 0.95E_{el}$. This result is in a remarkably good agreement with the experimentally observed drop in the elastic constants (see Introduction).

As to the full stress-strain curves, the quasireversible segments conspire with the avalanche plateaus to yield on the average a power response curve. The second main question was about the thermodynamical limit in the 2D system, which is achieved by both a convergent mean and a vanishing variance of the stress for $\gamma \lesssim 1$. In this region, we observed also the analog of the size-effect, as found in micropillars [2]. For the largest strains, the thermodynamical limit is not reached and we do not consider our simulations as conclusive there.

Our study opens a series of questions. The results on the quasireversible behavior between avalanches call for more detailed investigations. In particular, a study of the size effect with 3D DDD simulations, although computationally highly demanding, should be considered, because in that case not only the dislocation configurations, but also the boundary conditions are more realistic. Furthermore, the statistical properties of the finite-size behavior are best characterized by distribution functions, among which here we only described that of the local effective plastic shear modulus, characterizing quasireversible regions. The distribution of the stresses is of obvious interest, and at avalanches are expected to be related to extreme statistics. A longstanding problem in this area is the transition to steady flow, wherein the absence of a single critical point, rather critical behavior for all strains, has been shown before [43], but a detailed study is still overdue. Carrying forth experiments on micropillars [15] with various sizes and their comparison to the prediction from simulations would be of immediate interest.

ACKNOWLEDGMENTS

Financial supports of the Hungarian Scientific Research Fund (OTKA) under Contract Nos. K-105335 and PD-105256, and of the European Commission under Grant Agreement No. CIG-321842 (StochPlast) are acknowledged.

[1] M.-C. Miguel, A. Vespignani, S. Zapperi, J. Weiss, and J.-R. Grasso, Nature (London) **410**, 667 (2001).
[2] M. D. Uchic, D. M. Dimiduk, J. N. Florando, and W. D. Nix, Science **305**, 986 (2004).
[3] M. D. Uchic, P. A. Shade, and D. M. Dimiduk, Annu. Rev. Mater. Res. **39**, 361 (2009).
[4] F. F. Csikor, C. Motz, D. Weygand, M. Zaiser, and S. Zapperi, Science **318**, 251 (2007).
[5] M. LeBlanc, L. Angheluta, K. Dahmen, and N. Goldenfeld, Phys. Rev. Lett. **109**, 105702 (2012).
[6] P. D. Ispánovity, L. Laurson, M. Zaiser, I. Groma, S. Zapperi, and M. J. Alava, Phys. Rev. Lett. **112**, 235501 (2014).
[7] D. M. Dimiduk, C. Woodward, R. LeSar, and M. D. Uchic, Science **312**, 1188 (2006).
[8] J. Weiss and D. Marsan, Science **299**, 89 (2003).
[9] M. Zaiser and N. Nikitas, J. Stat. Mech. (2007) P04013.
[10] A. W. Lawson, Phys. Rev. **60**, 330 (1941).
[11] J. D. Eshelby, Proc. R. Soc. London, Ser. A **197**, 396 (1949).
[12] H. Ledbetter and S. Kim, Mat. Sci. Eng. A **101**, 87 (1988).
[13] A. B. Lebedev, Yu. A. Burenkov, S. A. Pulnev, V. V. Vetrov, and V. I. Kopylov, J. Phys. IV France **06**, C8-365 (1996).
[14] P. D. Ispánovity, I. Groma, G. Györgyi, F. F. Csikor, and D. Weygand, Phys. Rev. Lett. **105**, 085503 (2010).
[15] P. D. Ispánovity, A. Hegyi, I. Groma, G. Györgyi, K. Ratter, and D. Weygand, Acta Mat. **61**, 6234 (2013).
[16] D. M. Dimiduk, M. D. Uchic, and T. A. Parthasarathy, Acta Mater. **53**, 4065 (2005).
[17] N. A. Fleck and J. W. Hutchinson, J. Mech. Phys. Solids **49**, 2245 (2001).
[18] M. E. Gurtin, J. Mech. Phys. Solids **50**, 5 (2002).
[19] I. Groma, F. Csikor, and M. Zaiser, Acta Mater. **51**, 1271 (2003).

[20] I. Groma, G. Györgyi, and B. Kocsis, Phys. Rev. Lett. **96**, 165503 (2006).
[21] A. Acharya, A. Roy, and A. Sawant, Scripta Mater. **54**, 705 (2006).
[22] J. Kratochvíl and R. Sedláček, Phys. Rev. B **77**, 134102 (2008).
[23] S. D. Mesarovic, R. Baskaran, and A. Panchenko, J. Mech. Phys. Solids **58**, 311 (2010).
[24] S. Sandfeld, T. Hochrainer, M. Zaiser, and P. Gumbsch, J. Mater. Res. **26**, 623 (2011).
[25] L. H. Poh, R. H. J. Peerlings, M. G. D. Geers, and S. Swaddiwudhipong, J. Mech. Phys. Solids **61**, 913 (2013).
[26] D. Balint, V. Deshpande, A. Needleman, and E. Van der Giessen, Mod. Sim. Mat. Sci. Eng. **14**, 409 (2006).
[27] P. Guruprasad and A. Benzerga, Phil. Mag. **88**, 3585 (2008).
[28] D. Weygand, M. Poignant, P. Gumbsch, and O. Kraft, Mat. Sci. Eng. **483–484**, 188 (2008).
[29] A. A. Benzerga, J. Mech. Phys. Solids **57**, 1459 (2009).
[30] V. Beato, M. Zaiser, and S. Zapperi, arXiv:1106.3444v1 [cond-mat.mtrl-sci].
[31] G. Tsekenis, N. Goldenfeld, and K. A. Dahmen, Phys. Rev. Lett. **106**, 105501 (2011).
[32] P. M. Derlet and R. Maaß, Philos. Mag. (2015).
[33] F. R. Nabarro, *Theory of Crystal Dislocations* (Clarendon, Oxford, 1967), Vol. 1.
[34] I. Groma and G. S. Pawley, Phil. Mag. A **67**, 1459 (1993).
[35] F. F. Csikor, M. Zaiser, P. D. Ispánovity, and I. Groma, J. Stat. Mech. (2009) P03036.
[36] L. Laurson, M.-Carmen. Miguel, and M. J. Alava, Phys. Rev. Lett. **105**, 015501 (2010).
[37] L. Laurson and M. J. Alava, Phys. Rev. Lett. **109**, 155504 (2012).
[38] I. Groma, Phys. Rev. B **57**, 7535 (1998).
[39] A. Borbély and I. Groma, Appl. Phys. Lett. **79**, 1772 (2001).
[40] I. Groma, D. Tüzes, and P. D. Ispánovity, Scripta Mater. **68**, 755 (2013).
[41] M.-Carmen. Miguel, A. Vespignani, M. Zaiser, and S. Zapperi, Phys. Rev. Lett. **89**, 165501 (2002).
[42] J. Rosti, J. Koivisto, L. Laurson, and M. J. Alava, Phys. Rev. Lett. **105**, 100601 (2010).
[43] P. D. Ispánovity, I. Groma, G. Györgyi, P. Szabó, and W. Hoffelner, Phys. Rev. Lett. **107**, 085506 (2011).
[44] M. Zaiser, M.-Carmen. Miguel, and I. Groma, Phys. Rev. B **64**, 224102 (2001).
[45] D. Dickel, K. Schulz, S. Schmitt, and P. Gumbsch, Phys. Rev. B **90**, 094118 (2014).
[46] P. M. Derlet and R. Maass, Modelling Simul. Mater. Sci. Eng. **21**, 035007 (2013).
[47] T. A. Parthasarathy, S. I. Rao, D. M. Dimiduk, M. D. Uchic, and D. R. Trinkle, Scripta Mater. **56**, 313 (2007).
[48] J. A. El-Awady, M. Wen, and N. M. Ghoniem, J. Mech. Phys. Solids **57**, 32 (2009).
[49] C. Motz, D. Weygand, J. Senger, and P. Gumbsch, Acta Mater. **57**, 1744 (2009).
[50] C. Zhou, I. J. Beyerlein, and R. LeSar, Acta. Mater. **59**, 7673 (2011).
[51] J. Senger, D. Weygand, C. Motz, P. Gumbsch, and O. Kraft, Acta Mater. **59**, 2937 (2011).
[52] D. Weygand, L. H. Friedman, E. V. d. Giessen, and A. Needleman, Model. Simul. Mater. Sc. **10**, 437 (2002).
[53] H. Mughrabi, Metall. Mater. Trans. B **40B**, 431 (2009).
[54] L. Kovács and L. Zsoldos, *Dislocations and Plastic Deformation* (Pergamon Press, Oxford, 1973).